Electronic Supplementary Material (ESI) for Chemical Communications

Highly Emissive Zn-Ln Metal Organic Frameworks with an Unusual 3D Inorganic Subnetwork

C. B. Liu,[†,!!] *R. A. S. Ferreira,*[‡] *F. A. A. Paz,*[†] *A. Cadiau,*[†] *L. D. Carlos,*[‡] *L. S. Fu,*[,‡] *J. Rocha,**[,†], *F.-N. Shi**[,†]

[†] Department of Chemistry, CICECO, University of Aveiro, 3810-193 Aveiro, Portugal,
[‡] Department of Physics, CICECO, University of Aveiro, 3810-193 Aveiro, Portugal
[!!] School of Chemistry & Chemical Engineering, Jiangsu University, 212013, P R China
E-mail: fshi@ua.pt; rocha@ua.pt;

Supporting Information

Table of Contents

1. Experimental

General characterization. Infrared spectra were recorded on a Mattson 7000 FT-IR spectrometer using KBr pellets (Figure S1). Elemental analyses for C, N, and H were performed with a CHNS-932 elemental analyzer at the Microanalysis Laboratory at the Department of Chemistry, University of Aveiro. Thermogravimetric analyses (TGA) were carried out using a Shimadzu TGA 50 under air, from room temperature to *ca*. 700 °C, with a heating rate of 5 °C/min. UV-visible diffuse reflectance spectra were measured on a JASCO V-560 instrument with each grounded solid samples from 200 nm to 800 nm under room temperature.

Morphological Characterization. Scanning electron microscopy (SEM) and energy dispersive analysis of X-ray spectroscopy (EDS) were performed using a Hitachi S-4100 field emission gun tungsten filament instrument working at 25 kV. EDS analysis were done on the single crystal particles and aggregated particles and confirmed the metal ratios of Zn : Ln ≈ 3 : 1 (Ln = La, Ce, Pr, Sm, Eu, Gd, Tb and Y) for all 8 compounds.

Powder X-ray Diffraction Studies. Powder X-ray diffraction (PXRD) data were collected at ambient temperature on a X'Pert MPD Philips diffractometer (Cu Kα X-radiation, λ = 1.54060 Å), equipped with a X'Celerator detector, a curved graphite-monochromated radiation and a flat-plate sample holder, in a Bragg-Brentano para-focusing optics configuration (40 kV, 50 mA). Intensity data were collected in the continuous scanning mode in the range ca. 5 ≦ 2θ□□≦ 50.

Powder X-ray Thermodiffraction Studies. The variable temperature experiments performed on **5** were conducted on the same instrument using a high-temperature Anton Parr HKL 16 chamber, controlled by a Anton Parr 100 TCU unit. Intensity data were collected in the step mode (0.02□, 5 s per step) in the range ca. 10 ≦ 2θ (º) ≦50 from room temperature to 500 ºC.

Synthesis. Chemicals were readily available from commercial sources and used as received without further purification: amorphous lanthanum (III) chloride heptahydrate ($LaCl_3 \cdot 7H_2O$, 99.9%, Fluka), cerium (III) chloride heptahydrate ($CeCl_3 \cdot 7H_2O$, 99.9%, Aldrich), praseodymium (III) chloride hexahydrate ($PrCl_3 \cdot 6H_2O$, 99.9%, Aldrich), samarium (III) chloride hexahydrate ($SmCl_3 \cdot 6H_2O$, 99%, Alfa Aesar), europium (III) chloride hexahydrate ($EuCl_3 \cdot 6H_2O$, 99.9%, Aldrich), lanthanide oxide (Sm_2O_3,

Eu_2O_3, Gd_2O_3, Tb_4O_7, 99.9%, Alfa Aesar), zinc acetate dihydrate ($Zn(CH_3COO)_2{\cdot}2H_2O$, 99%, Panreac), cadmium acetate dehydrate ($CdC_4H_6O_4{\cdot}2H_2O$, ≤98.0%, Fluka), 3,5-pyrazoledicarboxylic acid monohydrate (H_3pdc, $C_5H_4N_2O_2{\cdot}H_2O$, 97%, Aldrich).

Usually, the hydrothermal reaction was performed in a 25 mL Teflon-lined stainless steel autoclave under autogenous pressure. A mixture of $Zn(CH_3COO)_2$ (0.3 mmol), $LnCl_3$ (0.1 mmol) and H_3pdc (0.2 mmol) in H_2O (10 mL) was sealed in a 25 mL Teflon-lined bomb at 150 ºC for 3 days. Transparent polyhedral crystals were recovered by filtration, washed by distilled water (3*50 mL), and air-dried (Yield: 34%, 40%, 38%, 47%, 32% and 39% based on H_3pdc for **1-5**, respectively).

Another synthetic method for producing large amount of pure phase samples was done as follows. $Zn(CH_3COO)_2$ (0.1316 g, 0.6 mmol), Ln_2O_3 (0.1 mmol, 0.0352 g for Eu_2O_3, 0.0362 g for Gd_2O_3, 0.0374 g for Tb_4O_7, 0.0226 g for Y_2O_3) and H_3pdc (0.1044 g, 0.6 mmol) were mixed in distilled water (20 g), stirred for half an hour to get homogeneous mixture with the molar ratio of Zn : Ln : H_3pdc : H_2O = 3 : 1 : 3 : 4500, and then were sealed in teflon-lined autoclaves (the volume: 40 mL), heated at 170 ºC for 3 days. Large amount particles were harvested by filtration and dried under ambient condition (yield: 85%, 82%, 78% and 80% based on H_3pdc for **5-8**, respectively).

Elemental analyses of 1-8. Elemental analysis: Calcd (%) for **1** $\{[Zn_3La(pdc)_3(H_2O)]{\cdot}0.25H_2O\}_n$ (MW = 816.77) : C 22.03, H 0.67, N 10.28; Found, C 21.89, H 0.89, N 10.23. Calcd (%) for **2** $\{[Zn_3Ce(pdc)_3(H_2O)]{\cdot}0.25H_2O\}_n$ (MW = 817.98) : C 22.00, H 0.67, N 10.26; Found, C 21.75, H 0.70, N 10.20. Calcd (%) for **3** $\{[Zn_3Pr(pdc)_3(H_2O)]{\cdot}0.25H_2O\}_n$ (MW = 818.77) : C 21.98, H 0.67, N 10.25; Found, C 21.68, H 0.87, N 10.31. Calcd (%) for **4** $\{[Zn_3Sm(pdc)_3(H_2O)]{\cdot}0.25H_2O\}_n$ (MW = 828.21) : C 21.73, H 0.66, N 10.14; Found, C 21.79, H 0.81, N 10.00. Calcd (%) for **5** $\{[Zn_3Eu(pdc)_3(H_2O)]{\cdot}0.25H_2O\}_n$ (MW = 829.82) : C 21.69, H 0.66, N 10.12; Found, C 21.40, H 0.76, N 9.69. Calcd (%) for **6** $\{[Zn_3Gd(pdc)_3(H_2O)]{\cdot}0.25H_2O\}_n$ (MW = 835.11) : C 21.55, H 0.65, N 10.05; Found, C 21.31, H 0.75, N 9.90. Calcd (%) for **7** $\{[Zn_3Tb(pdc)_3(H_2O)]{\cdot}0.25H_2O\}_n$ (MW = 836.78) : C 21.51, H 0.65, N 10.03; Found, C 21.33, H 0.55, N 9.87. Calcd (%) for **8** $[Zn_3Y(pdc)_3(H_2O)]_n$ (MW = 762.27) : C 23.61, H 0.66, N 11.02; Found, C 23.37, H 0.67, N 10.86.

Selected FT-IR data (KBr pellets, ν/cm^{-1}) (Fig. S3): for **1**, 437 (w), 605 (w), 633 (w), 778 (m), 846 (m), 1021 (m), 1059 (m), 1218 (w), 1355 (s), 1402 (m), 1538 (s), 1577 (s), 1630 (s), 3161 (w), 3458 (w, br); for **2**, 434 (w), 594 (w), 635 (w), 778 (m), 853 (m), 1014 (m), 1052 (m), 1214 (w), 1363 (s), 1410 (m), 1533 (s), 1585 (s), 1632 (s), 3152 (w), 3453 (w, br); for **3**, 434 (w), 595 (w), 632 (w), 775 (m), 853 (m), 1014 (m), 1060 (m), 1218 (w), 1361 (s), 1412 (m), 1531 (s), 1577 (s), 1631 (s), 3153 (w), 3441 (m, br); for **4**, 437 (w), 587 (w), 632 (w), 770 (m), 853 (m), 1021 (m), 1051 (m), 1211 (w), 1371 (s), 1410 (m), 1531 (s), 1577 (s), 1630 (s), 3152 (w), 3449 (m, br); for **5**, 437 (w), 589 (w), 640 (w), 778 (m), 848 (m), 1013 (w), 1061 (m), 1213 (w), 1364 (s), 1415 (m), 1539 (s), 1585 (s), 1630 (s), 3154 (w), 3464 (w, br); for **6**, 436 (w), 587 (w), 640 (w), 776 (m), 854 (m), 1020 (m), 1056 (m), 1218 (w), 1365 (s), 1410 (m), 1539 (s), 1584 (s), 1612 (s), 3456 (w, br); for **7**, 436 (w), 595 (w), 640 (w), 776 (m), 851 (m), 1018 (w), 1063 (m), 1220 (w), 1371 (s), 1418 (m), 1539 (s), 1576 (s), 1629 (s), 3472 (w, br); for **8**, 444 (w), 595 (w), 642 (w), 776 (m), 851 (m), 1018 (m), 1060 (m), 1214 (m), 1365 (s), 1426 (m), 1531 (s), 1574 (s), 1629 (s), 3162 (w), 3484 (w, br).

Photoluminescence spectroscopy. The photoluminescence spectra were recorded at room temperature with a modular double grating excitation spectrofluorimeter with a TRIAX 320 emission monochromator (Fluorolog-3, Horiba Scientific) coupled to a R928 Hamamatsu photomultiplier. The spectra were acquired using the front face mode, and were corrected for detection and optical spectral response. Emission was corrected for the spectral response of the monochromators and the detector using typical correction spectrum provided by the manufacturer and the excitation spectra were corrected for the spectral distribution of the lamp intensity using a photodiode reference detector. The emission decay curves were acquired at room temperature with the setup described for the photoluminescence spectra using a pulsed Xe-Hg lamp (6 μs pulse at half width and 20-30 μs tail).

Absolute emission quantum yields. The absolute emission quantum yields were measured at room temperature using a quantum yield measurement system C9920-02 from Hamamatsu with a 150 W Xenon lamp coupled to a monochromator for wavelength discrimination, an integrating sphere as sample

chamber and a multi channel analyzer for signal detection. Three measurements were made for each sample so that the average value is reported. The method is accurate to within 10 %.

X-Ray crystallography. Complete single-crystal data of compounds **1-5 & 7** were collected at 150(2) K (**6** & **8** were collected at 296 K) on a Bruker X8 Kappa APEX II charge-coupled device (CCD) area-detector diffractometer (Mo-Kα graphite monochromated radiation, λ = 0.7107 Å) controlled by the APEX2 software package [1] and equipped with an Oxford Cryosystems Series 700 cryostream monitored remotely by using the software interface Cryopad [2]. Images were processed using the software package SAINT+ [3]. Absorption corrections were applied by the multiscan semiempirical method implemented in SADABS [4]. The structures were solved by direct method using SHELXS-97 [5] and refined using SHELXL-97 [6]. All non-hydrogen atoms were successfully refined with anisotropic displacement parameters. Hydrogen atoms bound to carbon were located at their idealized positions by employing the HFIX 43 instruction in SHELXL-97 and included in subsequent refinement cycles in riding motion approximation with isotropic thermal displacement parameters (Uiso) fixed at 1.2Ueq of the carbon atom to which they were attached. The hydrogen atoms associated with water molecules were visible in the last difference Fourier maps synthesis. These atoms have been included in the final structural models with the O-H distances restrained to 0.85(1) Å, in order to ensure a chemically reasonable geometry for these moieties, and with Uiso fixed at 1.2Ueq of the parent oxygen atoms. The detailed crystallographic data and structural refinement parameters have been summarized in Table S1. The selected bond distances and angles were listed in Table S2. Complete crystallographic data for the structure reported in this paper have been deposited in the CIF format with the Cambridge Crystallographic Data Center as supplementary publication no. CCDC 869773 - 869780. Copies of the data can be obtained free of charge on application to CCDC, 12 Union Road, Cambridge CB2 1EZ, UK (fax: (44) 1223336-033; e-mail: deposit@ccdc.cam.ac.uk).

2. Coordination Mode of pdc Ligand

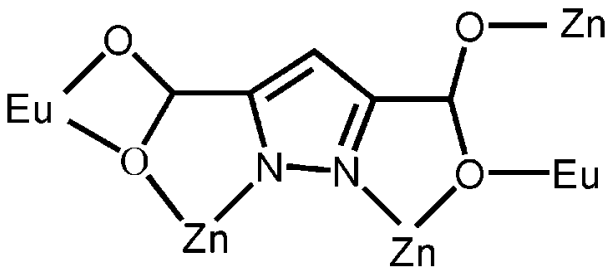

Scheme 1. pdc ligand and its coordination mode in this framework.

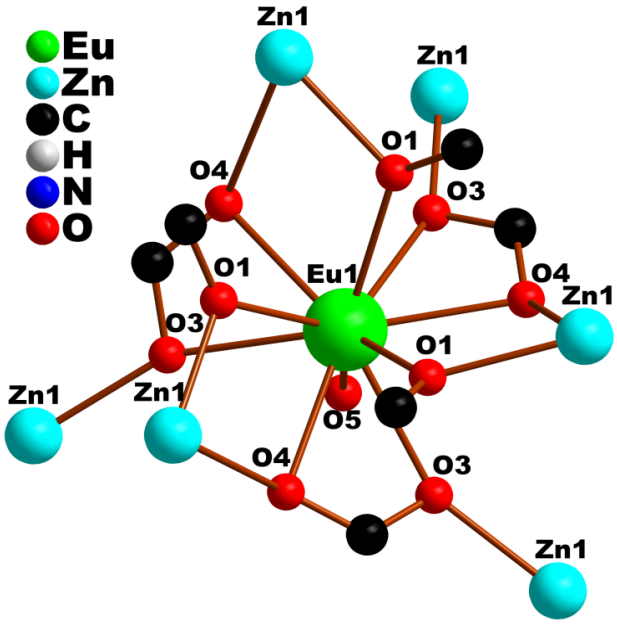

Figure S1. The coordination sphere of lanthanide ion, $[EuO_{10}]$ fragment further linking 6 Zn^{2+} ions via bridging oxygen atoms (O1, O3 & O4).

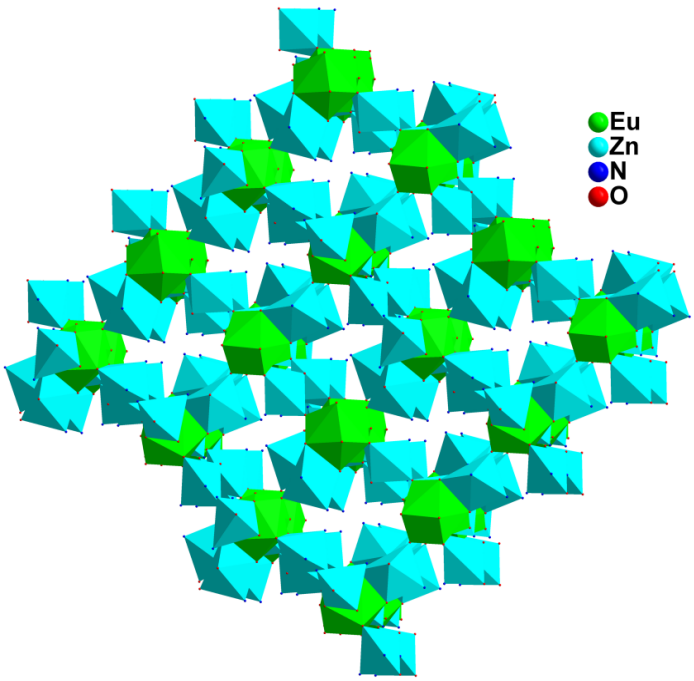

Figure S2. The super-cell (2×2×2) framework shows truly 3-dimensional inorganic subnetwork of Ln-O-Zn as a unique feature for this structure. C, H atoms and N-N bonds are omitted so that the infinite framework exhibits Ln-O-Zn 3D inorganic connectivity.

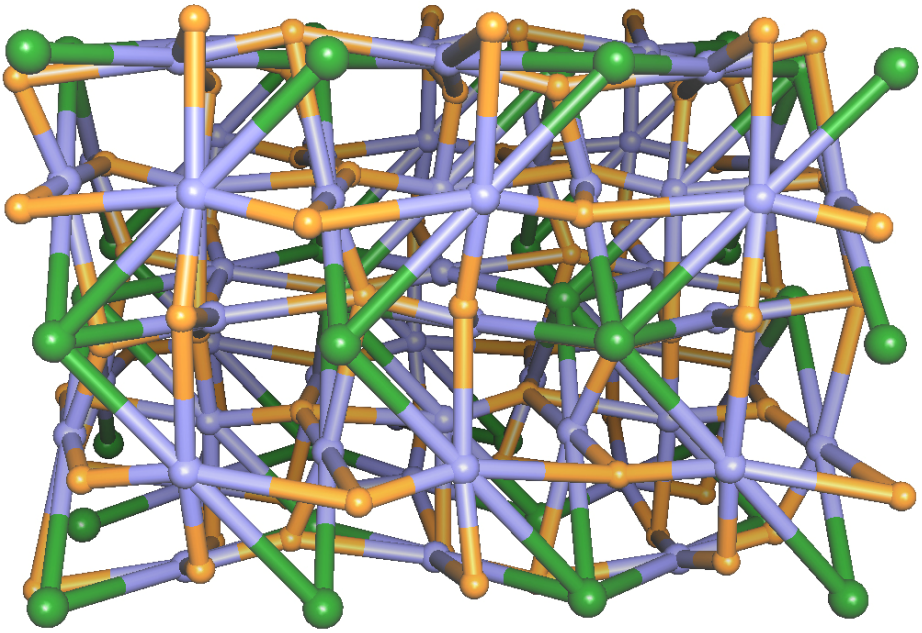

Figure S3. Topological representation of the mixed-metal 3*d*-4*f* $\{[Zn_3Ln(pdc)_3(H_2O)]\cdot 0.125H_2O\}_n$ MOF materials as a trinodal 4,6,6-connected network with total Schäfli symbol $\{4^3.6^3\}_3\{4^3.6^9.8^3\}_3\{4^9.6^6\}$. Nodes: ● lanthanide cation; ● Zn^{2+}; ● centre of gravity of pdc^{3-}.

3. SEM Images

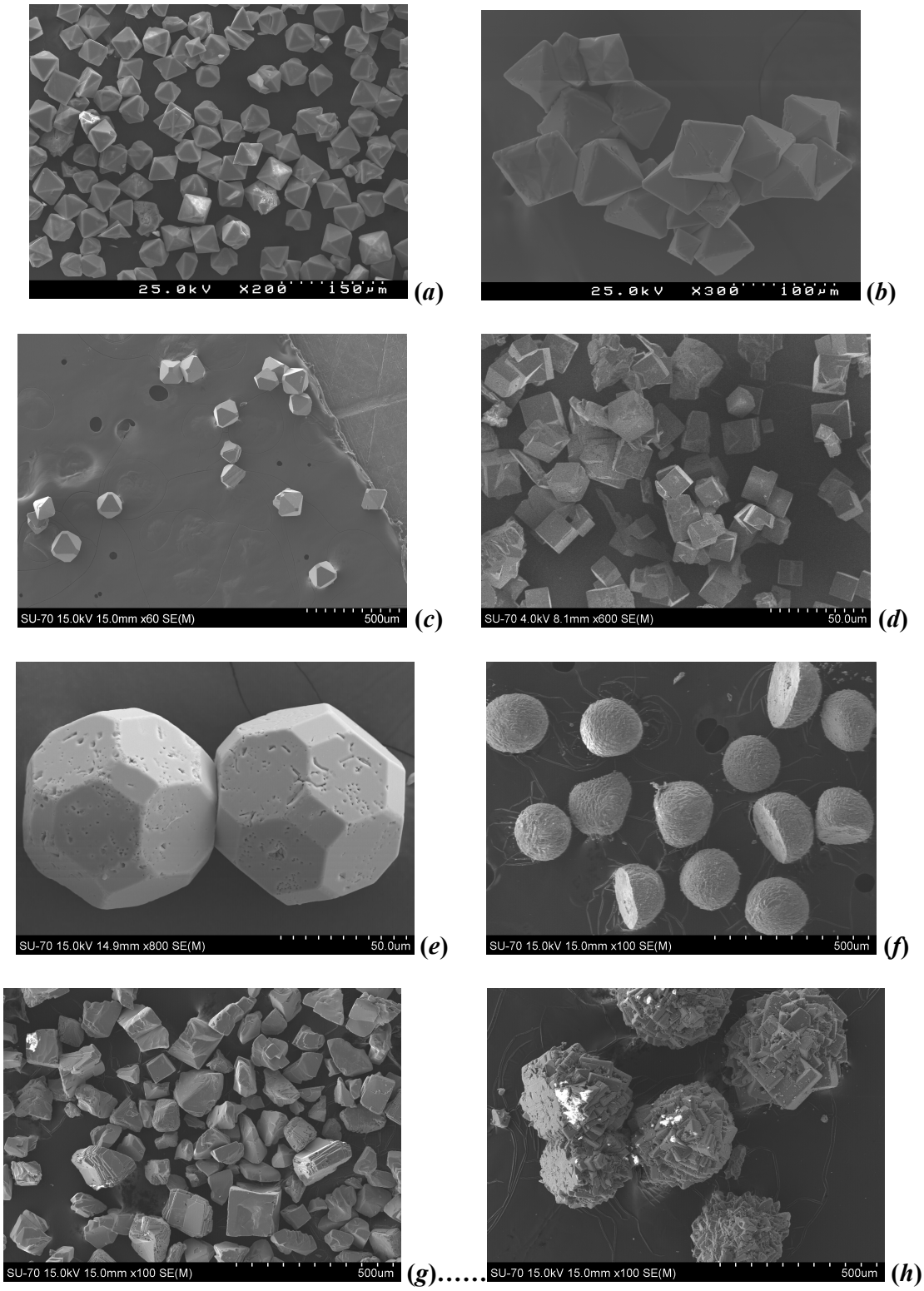

Figure S4. SEM images show the rich particle morphologies. **(*a*): 1; (*b*) : 2 ; (*c*) : 3 ; (*d*) : 4 ; (*e*): 5; (*f*): 6 ; (*g*): 7 ; (*h*): 8.**

4. FT-IR Spectra

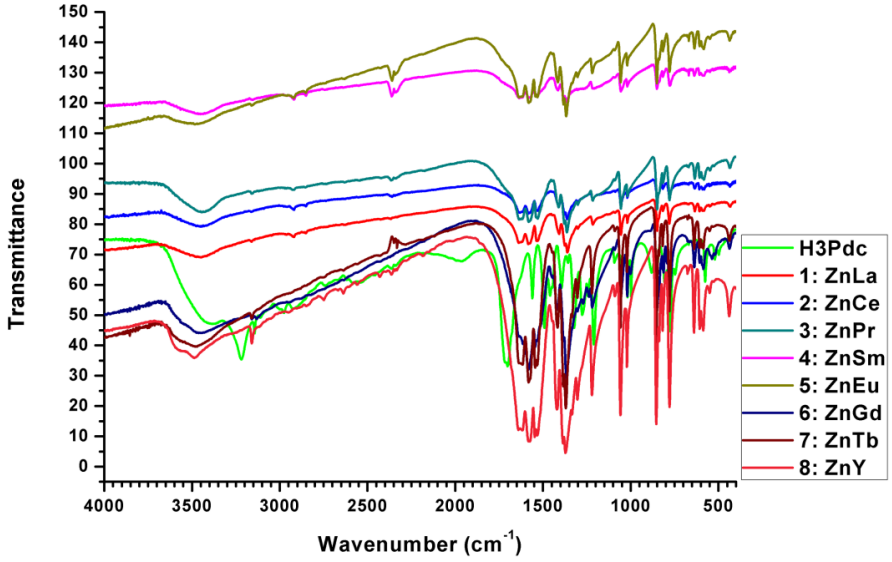

Figure S5. FT-IR spectra of the H_3pdc ligand and MOFs **1-8**

5. TGA Plots in Air

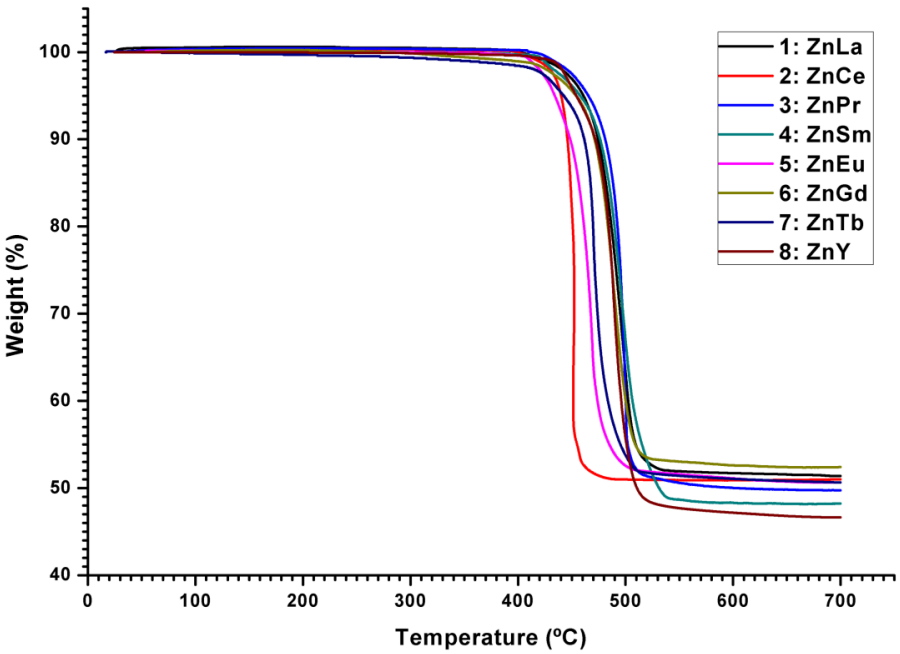

Figure S6. TGA plots of the CPs **1-8** show the similar thermal behaviors (decomposed after 400 ºC) in this framework.

6. Powder XRD Patterns of Bulk Samples

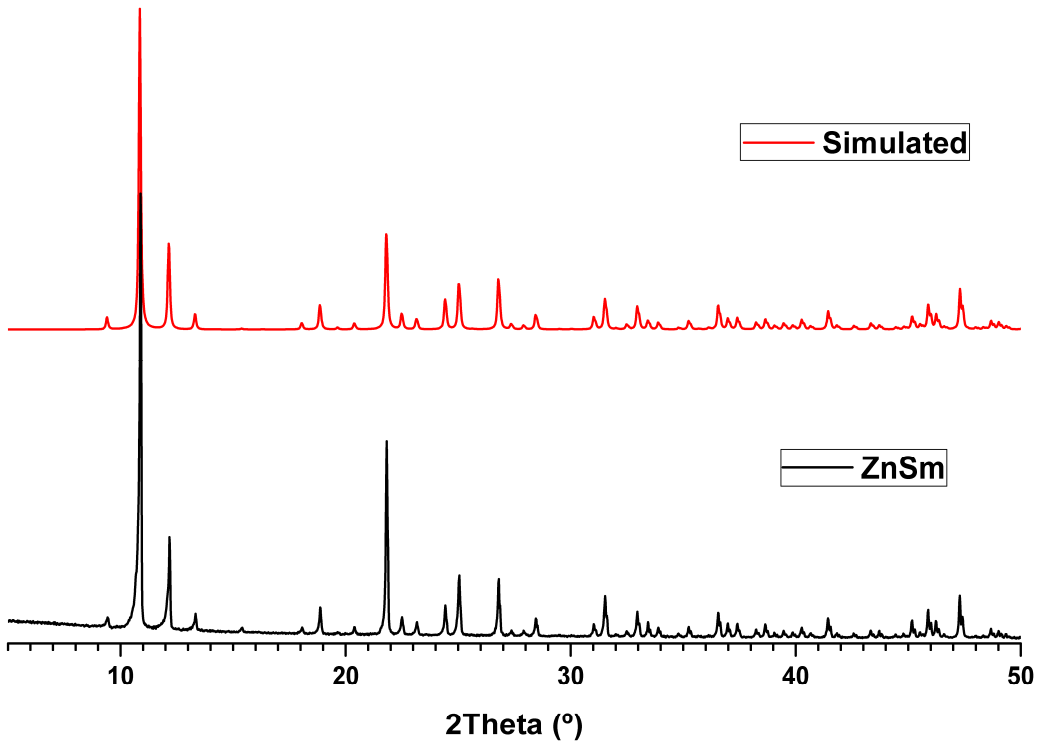
Simulated
ZnSm
10
20
30
40
50
2Theta (°)

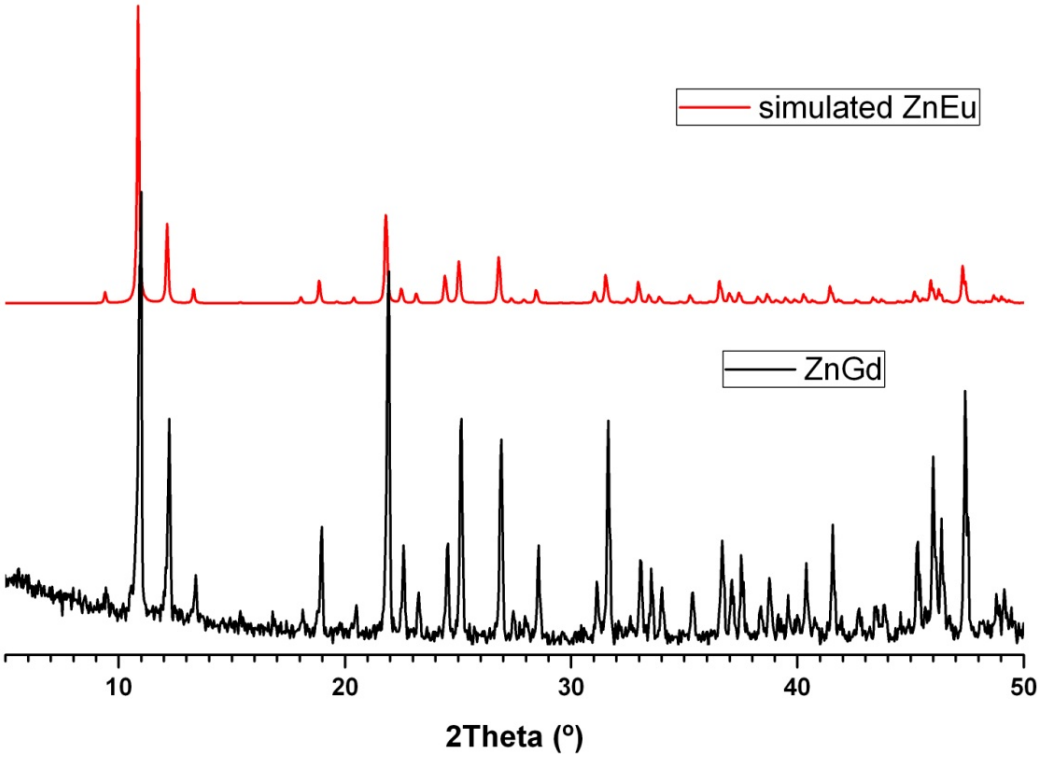
simulated ZnEu
ZnGd
10
20
30
40
50
2Theta (°)

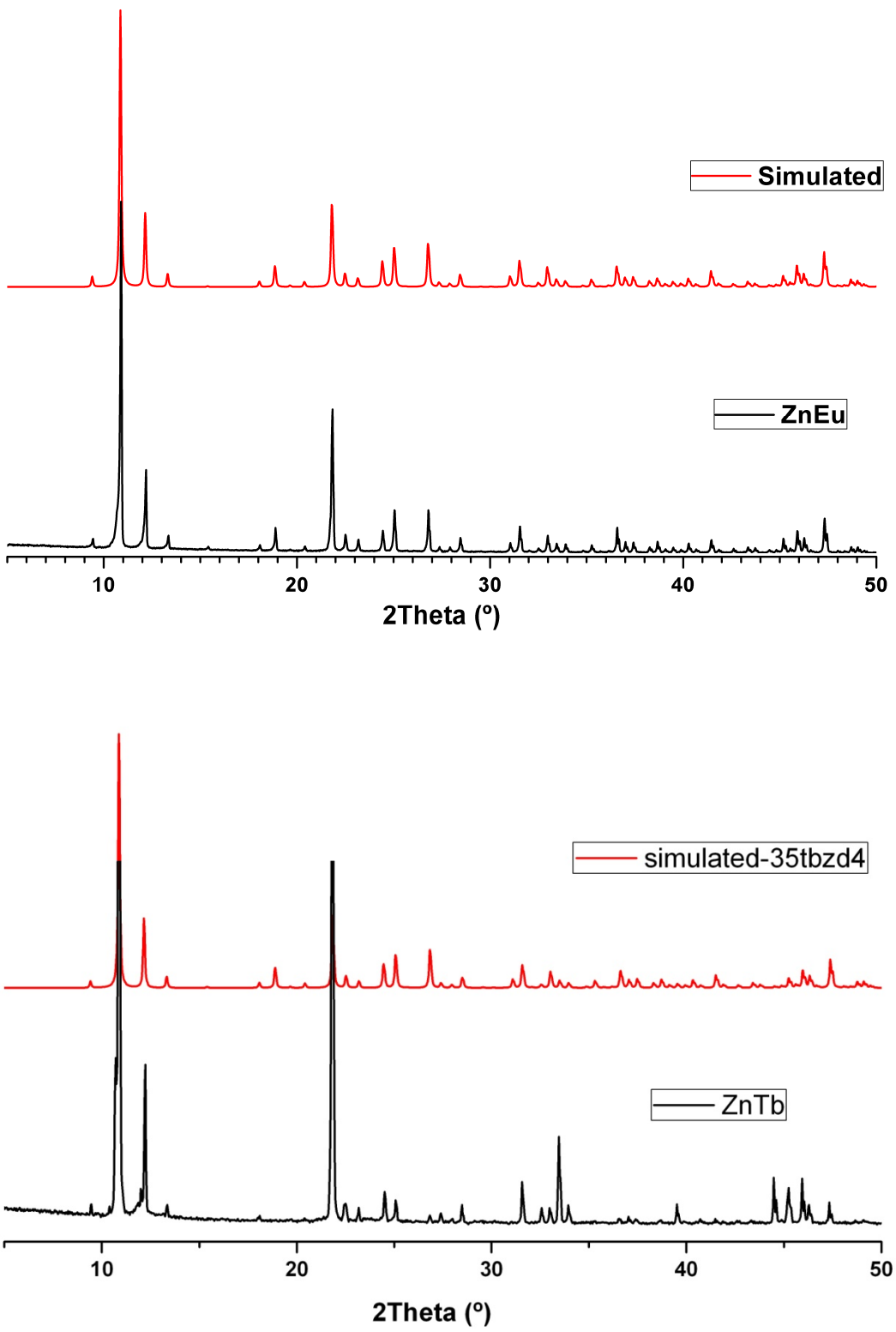

Figure S7. Powder XRD patterns of some samples compared with the ones from their single crystal structure data.

7. In situ Powder XRD Pattern of (5)

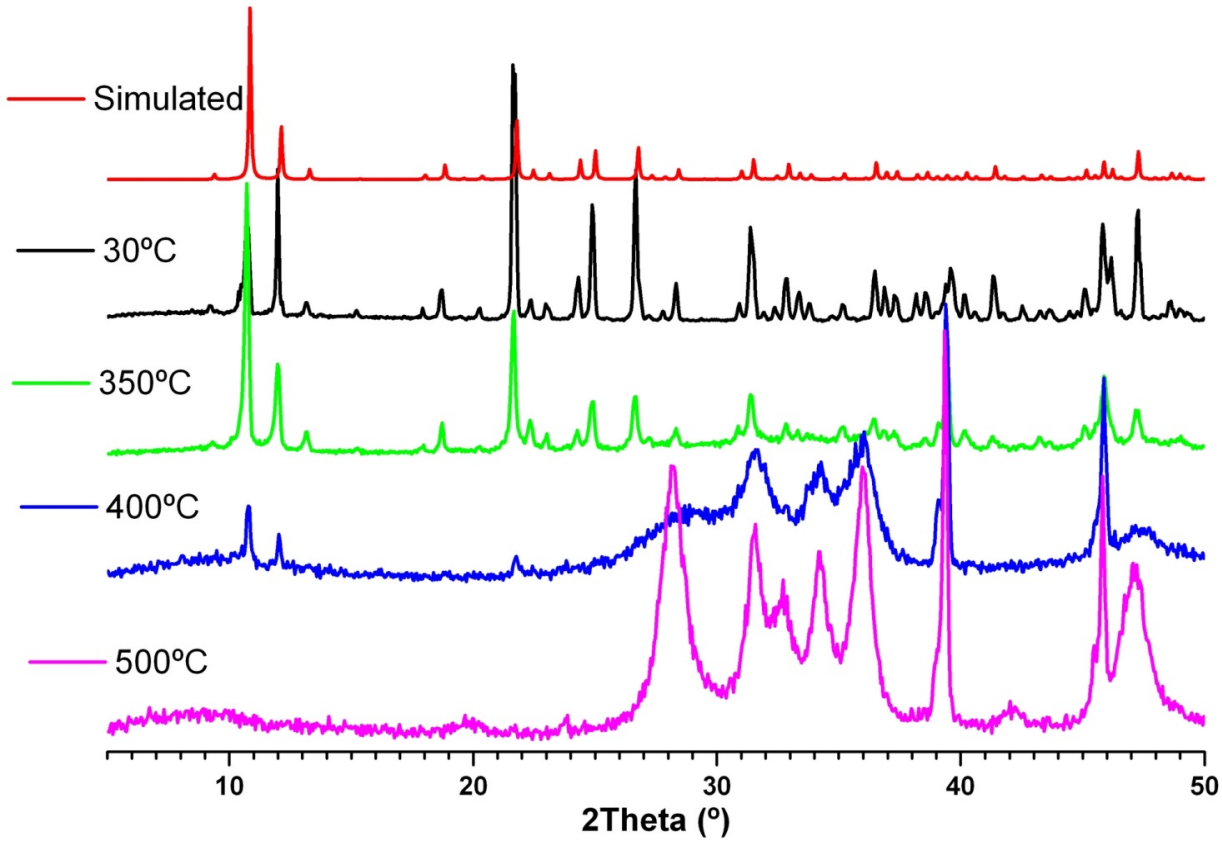

Figure S8. In situ Powder XRD pattern of **5** in air indicate the framework is thermally stable up to at least 350ºC. The compound **5** starts to decompose at 400 ºC and dense phases appear. At 500 ºC, the cubic framework completely disappears and the dense phases become clear suggesting that **5** has been decomposed into three phases: Eu_2O_3, ZnO and $ZnEu_2O_4$ which are confirmed by the comparison of current powder XRD data with those of Eu_2O_3, ZnO and $ZnEu_2O_4$ from the database.

8. Photoluminescence Properties& UV/VIS/NIR Absorption Spectra

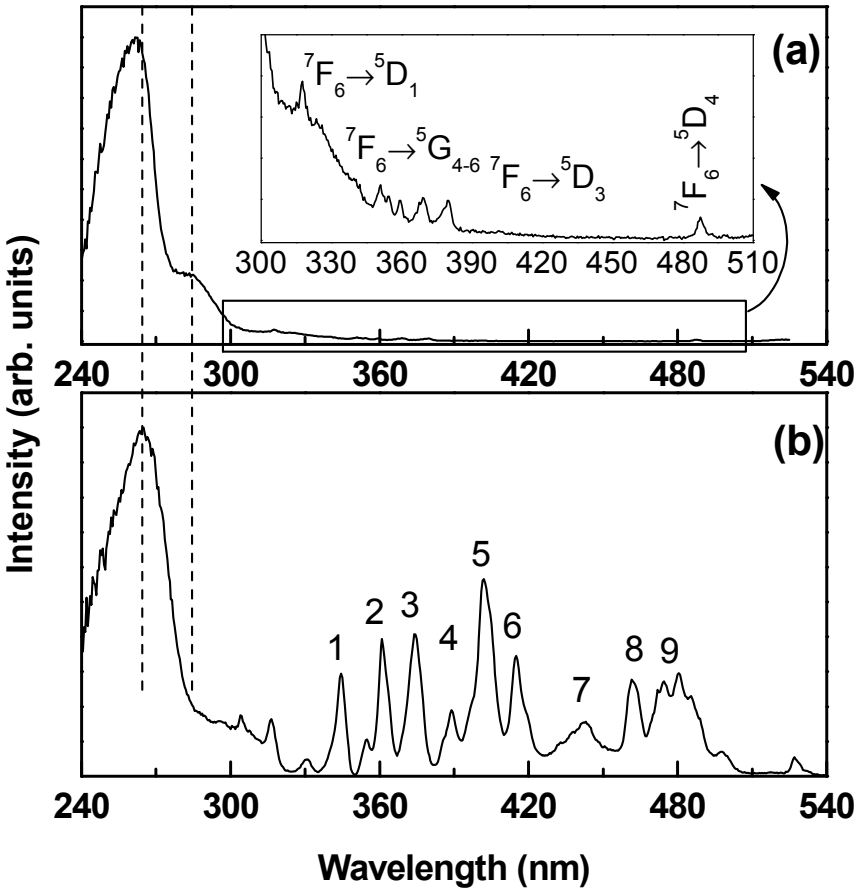

Fig. S9 Excitation spectra (at 300 K) of (a) 7 and (b) 4 monitored at 542 and 641 nm, respectively. The inset in (a) shows a magnification (×100) of the intra-4f^8 transition. In (c) Sm^{3+}-related transitions involving the ^{6}H5/2 level and the excited states are depicted as (1) $^4H_{9/2}$, $^4D_{7/2}$; (2) $^4D_{3/2}$, $^4P_{5/2}$; (3) ^{4}D1/2, $^4L_{17/2}$, $^6P_{7/2}$; (4) $^4H_{11/2}$, $^4M_{15/2,21/2}$, $^4G_{11/2}$; (5) $^6P_{3/2}$, $^4F_{7/2}$, $^4L_{13/2}$; (6) $^4M_{19/2}$, $^6P_{5/2}$; (7) $^4I_{15/2}$, $^4G_{9/2}$, $^4M_{17/2}$; (8) $^4I_{13/2}$ and (9) $^4I_{9/2}$.

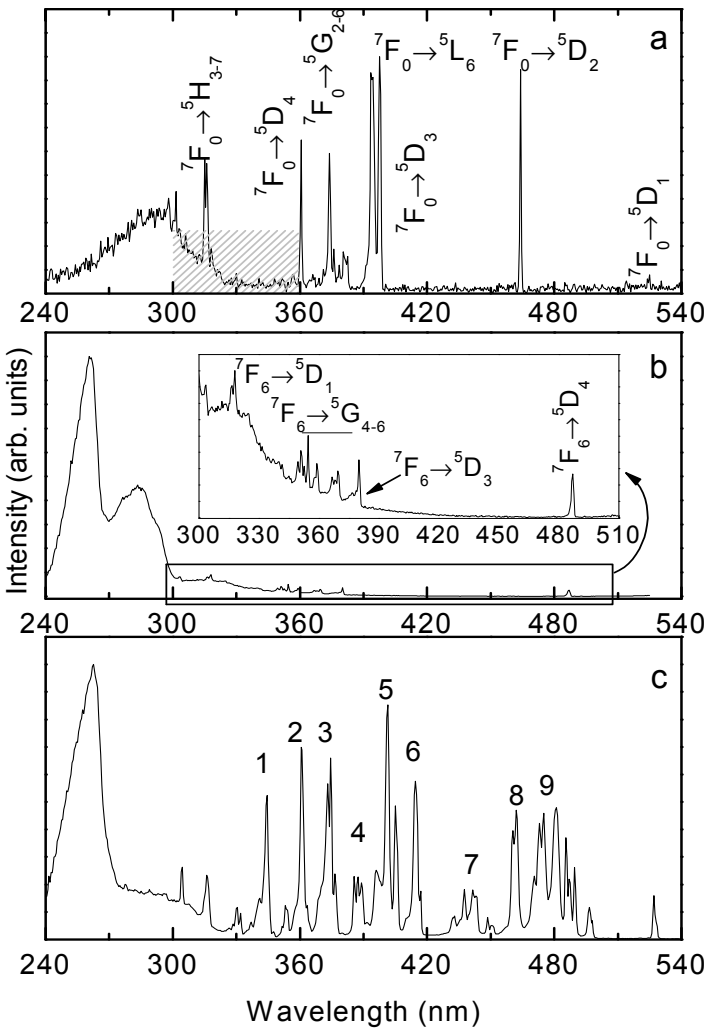

Figure S10 Excitation spectra measured at 10 K of (a) EuZn, (b) TbZn and (c) SmZn materials monitored at 618, 542 and 641 nm, respectively. The inset in (b) shows a magnification (×100) of the intra-4f[8] transition between 300 and 510 nm. For clarity, the Sm^{3+}-related transitions in (c) involving the $^6H_{5/2}$ level and the excited states are depicted as (1) $^4H_{9/2}$, $^4D_{7/2}$, (2) $^4D_{3/2}$, $^4P_{5/2}$, (3) $^4D_{1/2}$, $^4L_{17/2}$, $^6P_{7/2}$, (4) $^4H_{11/2}$, $^4M_{15/2,}$ $_{21/2}$, $^4G_{11/2}$ (5) $^6P_{3/2}$, $^4F_{7/2}$, $^4L_{13/2}$, (6) $^4M_{19/2}$, $^6P_{5/2}$, (7) $^4I_{15/2}$, $^4G_{9/2}$, $^4M_{17/2}$, (8) $^4I_{13/2}$ and (9) $^4I_{9/2}$.

The excitation paths for each crystal were also investigated at 10 K (Figure S10). The low-temperature excitation spectra of the Tb^{3+} and Sm^{3+}-containing crystals resemble those acquired at 300 K, apart from a decrease in the *fwhm* of all the transitions and an increase in the relative intensity of the intra-4f lines. The excitation spectrum of the Eu-Zn reveals an increase in the relative intensity of the pdc-related and LMCT bands with respect to that of the intra-4f lines.

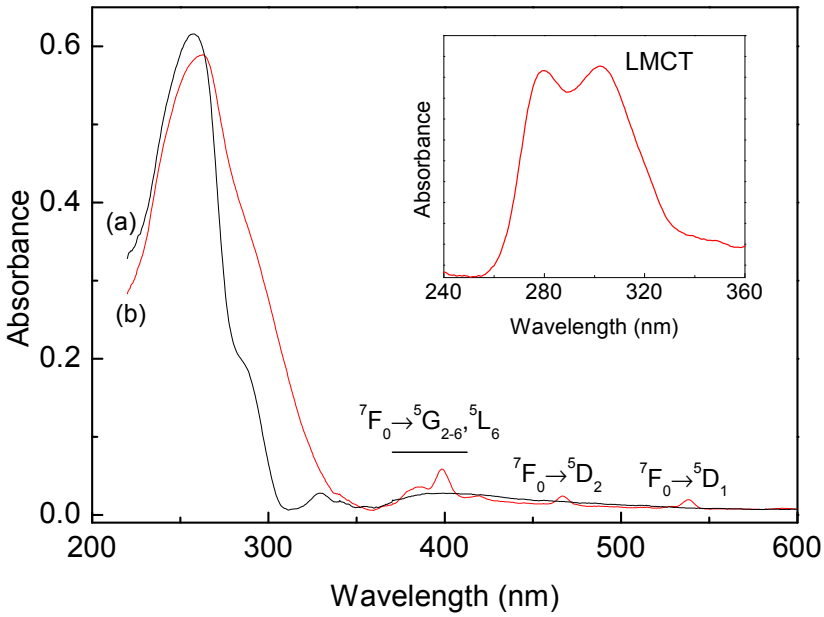

Figure S11. Diffuse reflectance spectra of (a) **5** (ZnEu) and (b) **6** (ZnGd). The inset shows the arithmetic difference between the two spectra between 200 and 380 nm.

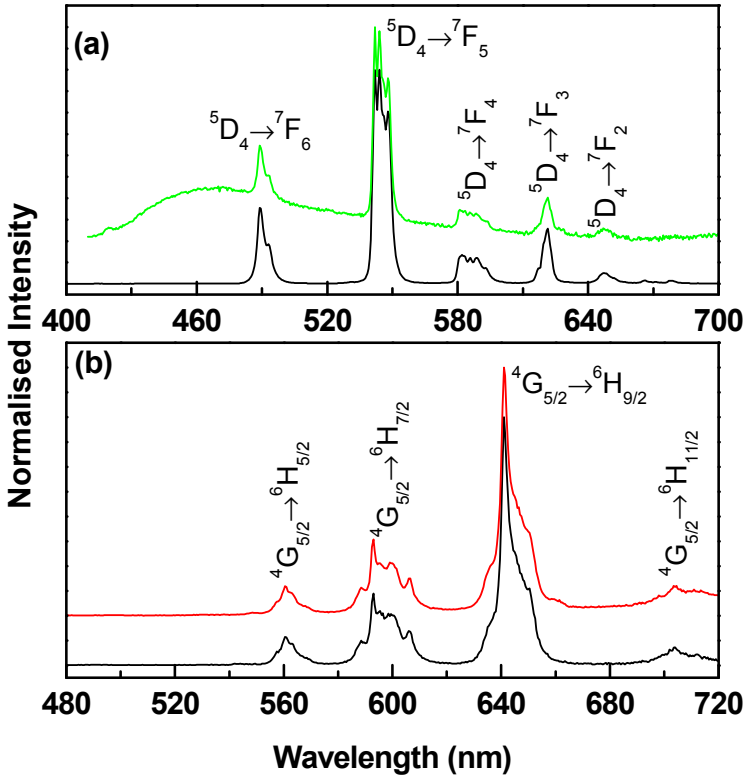

Fig. S12 Emission spectra (300 K) of (a) 7, (b) 4 excited at 260–280 (black), 380 (green), 401 (red) nm.

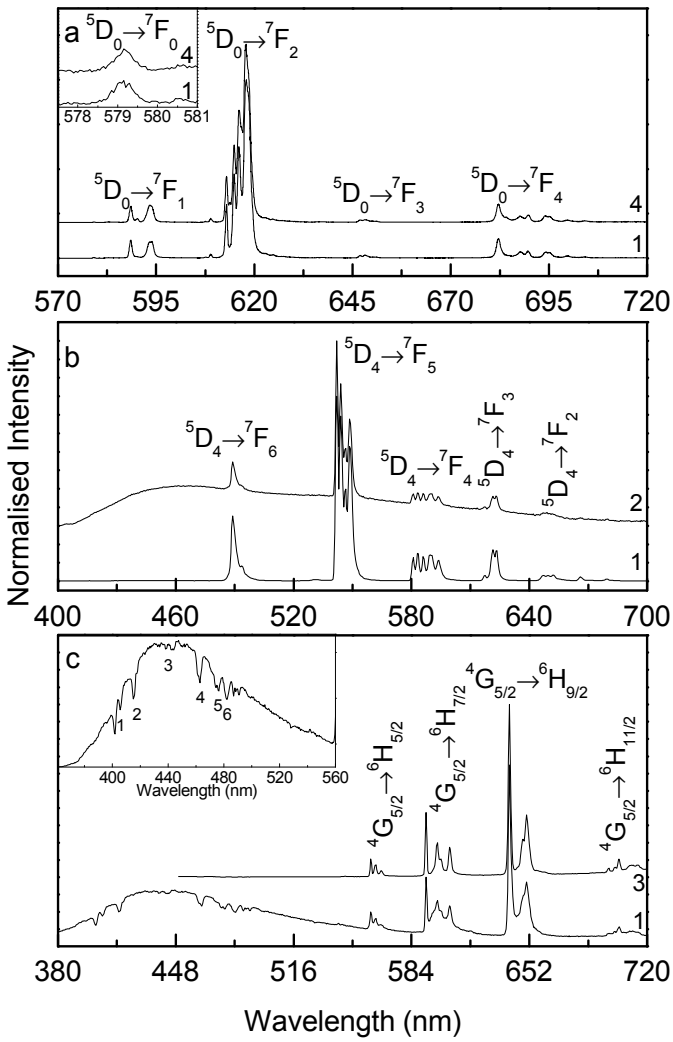

Figure S13 Emission spectra acquired at 10 K of (a) EuZn, (b) TbZn and (c) SmZn excited at (1) 260-280 nm, (2) 380 nm, (3) 401 nm, (4) 465 nm. The insets show a magnification of the (a) intra-4f^6 $^5D_0 \rightarrow {}^7F_0$ transition and (c) pdc-related emission overlapped by a series of intra-4f^5 self-absorptions between the $^4G_{5/2}$ level and the excited states (1) $^6P_{3/2}$, $^4F_{7/2}$, $^4L_{13/2}$, (2) $^4M_{19/2}$, $^6P_{5/2}$, (3) $^4I_{15/2}$, $^4G_{9/2}$, $^4M_{17/2}$, (4) $^4I_{13/2}$ and (5) $^4I_{9/2}$.

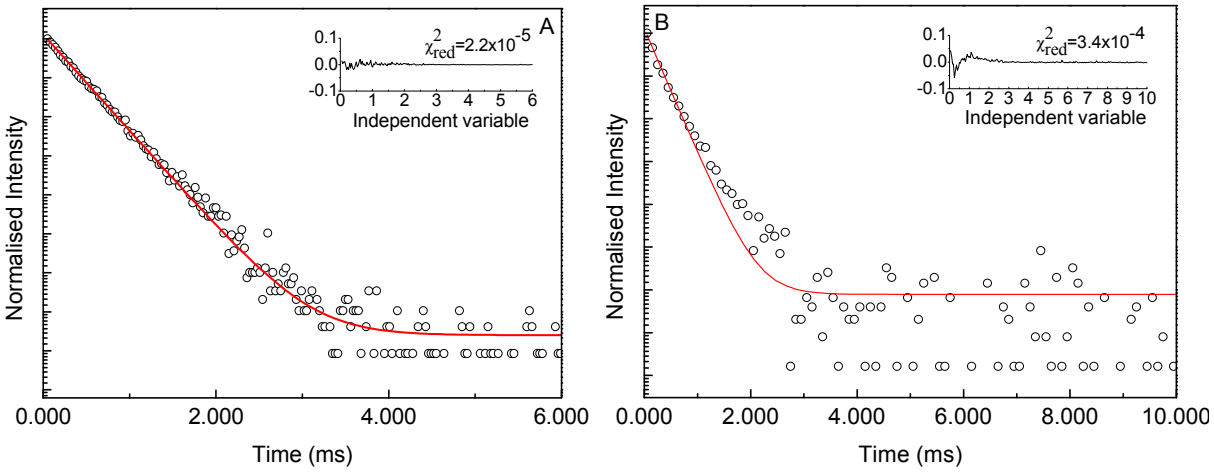

Figure S14 Emission decay curves acquired at 300 K of (A) ZnEu monitored at 614 nm and excited at 393 nm and (B) ZnTb monitored at 542 nm and excited at 260 nm. The solid lines correspond to the data best fit using a single exponential function. The insets show the respective regular residual plots and the χ^2_{red} values for a better judgment of the fits quality.

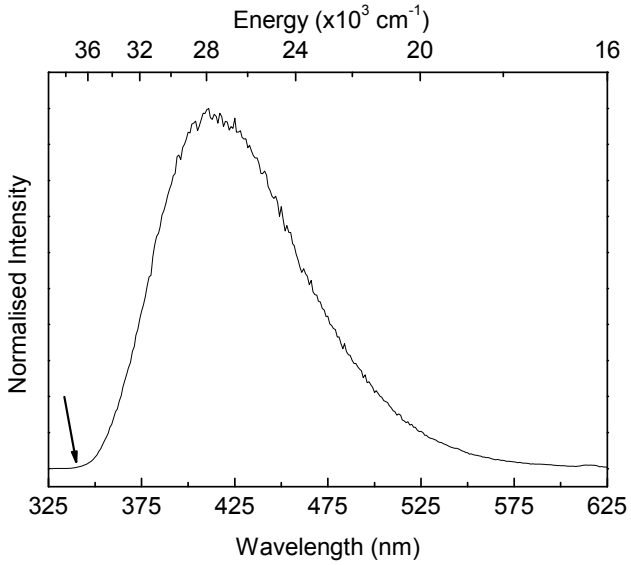

Figure S15. Time-resolved emission spectrum (12 K) of **6** (ZnGd) excited at 270 nm and acquired with a starting delay of 0.05 ms and an integration window of 20.00 ms.

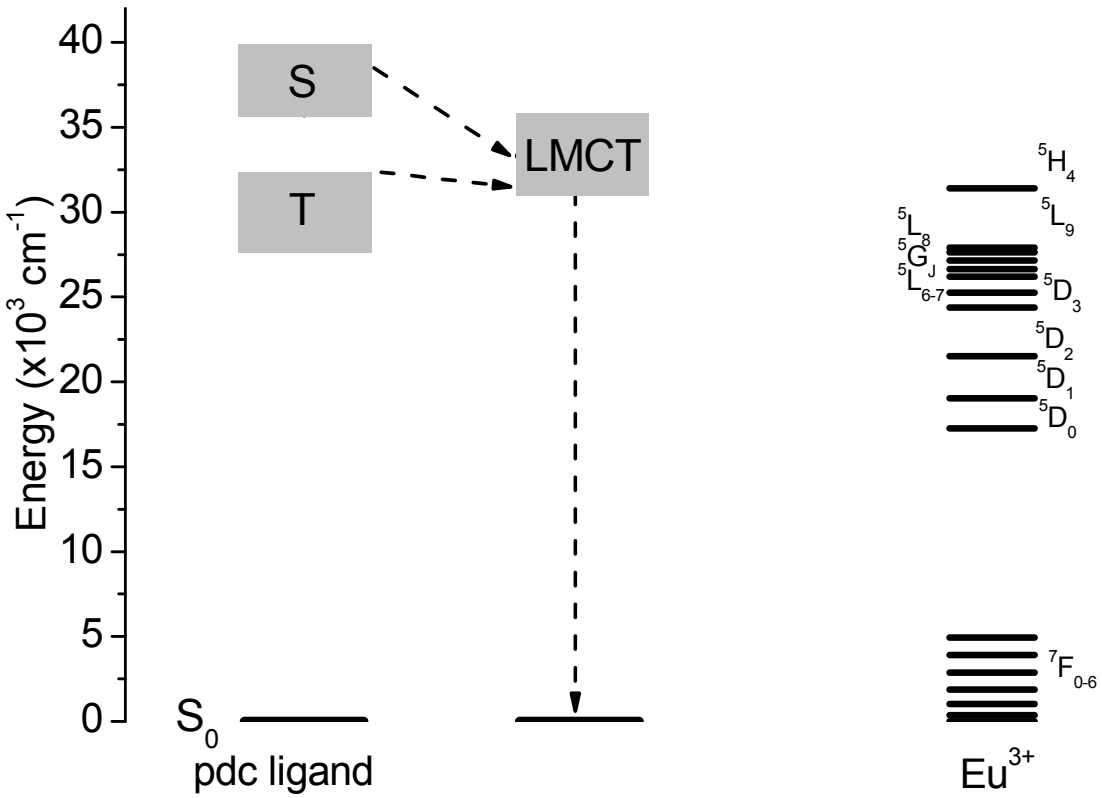

Figure S16. Partial energy level diagram for **5** (ZnEu). The width of the S, T and LMCT were estimated from the fwhm estimated from the diffuse reflectance (S, LMCT, Figure S10) and emission (T, Figure S13) spectra of **6** (ZnGd). The dashed arrows represent possible non-radiative energy transfer paths.

The energies of the pdc ligand singlet excited state was determined from the diffuse reflectance spectrum of GdZn (Figure S11). Under UV/Vis excitation, the GdZn complex displays a long-lived (10^{-3} s time scale) broad band emission ascribed to the triplet state of the pdc ligand (Figure S15), enabling the determination of the energy of the triplet state (arrow in Figure S15). The experimental energy values for the singlet (*ca.* 265 nm, 37736 cm^{-1}), triplet (*ca.* 340 nm, 29413 cm^{-1}) and LMCT (*ca.* 300 nm, 33333 cm^{-1}) states were used to set up the left part of the diagram shown on Figure S16. The LMCT state fall in the same energy range as the ligand singlet/triplet states, interfering with efficient energy transfer from ligands-to-Eu^{3+}.

9. Tables of Crystal Structure Data (Table 1 & 2)

Table 1 Crystal Data Collection and Refinement Details for {[$Zn_3Ln(pdc)_3(H_2O)]\cdot 0.25H_2O$}n (Ln = La, 1; Ce, 2; Pr, 3; and Sm, 4.

	1	2	3	4
formula	$C_{15}H_{5.50}LaN_6O_{13.25}Zn_3$	$C_{15}H_{5.50}CeN_6O_{13.25}Zn_3$	$C_{15}H_{5.50}PrN_6O_{13.25}Zn_3$	$C_{15}H_{5.50}SmN_6O_{13.25}Zn_3$
formula weight	816.77	817.98	818.77	828.21
temperature/ K	150(2)	150(2)	150(2)	150(2)
crystal type	white cube	white cube	white block	white cube
crystal size/mm	0.04 x 0.04 x 0.04	0.06 x 0.06 x 0.06	0.16 x 0.14 x 0.10	0.08 x 0.08 x 0.08
crystal system	cubic	cubic	cubic	cubic
space group	Pa-3	Pa-3	Pa-3	Pa-3
$a = b = c$/Å	16.3969(2)	16.3614(5)	16.3504(2)	16.30280(10)
$\alpha = \beta = \gamma$/°	90	90	90	90
volume/ Å^3	4408.44(9)	4379.9(2)	4371.04(9)	4332.98(5)
Z	8	8	8	8
$\rho_{calculated}$/g cm^{-3}	2.461	2.481	2.488	2.539
μ/mm^{-1}	5.209	5.371	5.528	6.038
θ range/□	3.04 to 29.15	3.52 to 30.50	3.74 to 30.49	3.75 to 30.50
completeness to theta	99.7%	99.6%	99.7%	99.8%
index ranges	$-13 \le h \le 21$, $-20 \le k \le 14$, $-22 \le l \le 22$	$-23 \le h \le 23$, $-22 \le k \le 22$, $-17 \le l \le 23$	$-14 \le h \le 23$, $-18 \le k \le 17$, $-22 \le l \le 13$	$-14 \le h \le 19$, $-23 \le k \le 16$, $-23 \le l \le 17$
collected reflections	13402	26397	23131	21914
independent reflections	1983 [R(int) = 0.0898]	2233 [R(int) = 0.0649]	2225 [R(int) = 0.0426]	2207 [R(int) = 0.0651]
final R indices [I □□$2\sigma(I)$]^{a,b}	R1 = 0.0451, wR2 = 0.0914	R1 = 0.0271, wR2 = 0.0530	R1 = 0.0239, wR2 = 0.0553	R1 = 0.0317, wR2 = 0.0611
final R indices (all data)^{a,b}	R1 = 0.0700, wR2 = 0.0996	R1 = 0.0397, wR2 = 0.0563	R1 = 0.0304, wR2 = 0.0576	R1 = 0.0495, wR2 = 0.0664
Goodness-of-fit on F^2	1.066	1.040	1.096	1.089
largest diff peak and hole/e Å^{-3}	1.294 and -1.240	0.778 and -0.929	0.846 and -0.869	0.767, -1.192
CCDC no.	CCDC 869773	CCDC 869774	CCDC 869775	CCDC 869776

[a] $R1 = \sum||Fo| - |Fc||/\sum|Fo|$; [b] $wR2 = \{\sum[w(Fo^2 - Fc^2)^2]/\sum[w(Fo^2)^2]\}^{1/2}$.

Table 1 (condinued) Crystal Data Collection and Refinement Details for {[$Zn_3Ln(pdc)_3(H_2O)]\cdot0.25H_2O$}n (Ln = Eu, 5; Gd, 6; Ln = Tb, 7) and [$Zn_3Y(pdc)_3(H_2O)$]n 8

	5	6	7	8
formula	$C_{15}H_{5.50}EuN_6O_{13.25}Zn_3$	$C_{15}H_{5.50}GdN_6O_{13.25}Zn_3$	$C_{15}H_{5.50}TbN_6O_{13.25}Zn_3$	$C_{15}H_5N_6O_{13}YZn_3$
formula weight	829.82	835.11	836.78	762.27
temperature/ K	150(2)	296(2)	150(2)	296(2)
crystal type	white cube	colorless cube	light brown stick	colorless cube
crystal size/mm	0.06 x 0.06 x 0.06	0.08 x 0.08 x 0.08	0.16 x 0.05 x 0.03	0.18 x 0.18 x 0.18
crystal system	cubic	cubic	cubic	cubic
space group	Pa-3	Pa-3	Pa-3	Pa-3
$a = b = c$/Å	16.29390(10)	16.29440(10)	16.2707(3)	16.2486(17)
$\alpha = \beta = \gamma$/°	90	90	90	90
volume/ Å^3	4325.89(5)	4326.29(5)	4307.44(14)	4289.9(8)
Z	8	8	8	8
$\rho_{calculated}$/g cm^{-3}	2.548	2.564	2.581	2.360
μ/mm^{-1}	6.233	6.399	6.631	6.079
θ range/□	3.54 to 30.51	3.54 to 27.86	2.80 to 30.47	2.80 to 33.18
completeness to theta	99.7%	99.8%	99.9%	99.7%
index ranges	$-17 \le h \le 23$, $-23 \le k \le 23$, $-23 \le l \le 23$	-20<=h<=14, -14<=k<=21, -10<=l<=18	-17<=h<=18, -22<=k<=9, -23<=l<=3	-24<=h<=25, -25<=k<=24, -22<=l<=20
collected reflections	54490	10474	9257	38823
independent reflections	2205 [R(int) = 0.0898]	1725 [R(int) = 0.0320]	2193 [R(int) = 0.0735]	2737 [R(int) = 0.0499]
final R indices [I □□$2\sigma(I)$][a,b]	R1 = 0.0267, wR2 = 0.0492	R1 = 0.0208, wR2 = 0.0443	R1 = 0.0349, wR2 = 0.0631	R1 = 0.0240, wR2 = 0.0568
final R indices (all data)[a,b]	R1 = 0.0492, wR2 = 0.0549	R1 = 0.0268, wR2 = 0.0461	R1 = 0.0554, wR2 = 0.0703	R1 = 0.0373, wR2 = 0.0609
Goodness-of-fit on F^2	1.038	1.099	1.059	1.096
largest diff peak and hole/e Å^{-3}	0.884, -0.695	0.439 and -0.590	0.929, -0.990	0.820, -0.365
CCDC no.	CCDC 869777	CCDC 869778	CCDC 869779	CCDC 869780

[a] $R1 = \sum||Fo| - |Fc||/\sum|Fo|$; [b] $wR2 = \{\sum[w(Fo^2 - Fc^2)^2]/\sum[w(Fo^2)^2]\}^{1/2}$.

Table 2. Selected Bond Distances (Å) and Angles (º) for 1-8

1			
La(1)-O(5)	2.554(10)	La(1)-O(4)#1	2.579(4)
La(1)-O(4)	2.579(4)	La(1)-O(4)#2	2.579(4)
La(1)-O(1)#3	2.592(4)	La(1)-O(1)#4	2.592(4)
La(1)-O(1)#5	2.592(4)	La(1)-O(3)#1	2.623(4)
La(1)-O(3)	2.623(4)	La(1)-O(3)#2	2.623(4)
Zn(1)-O(2)#6	2.007(4)	Zn(1)-N(2)	2.033(5)
Zn(1)-N(1)#7	2.081(5)	Zn(1)-O(3)	2.122(4)
Zn(1)-O(1)#7	2.156(4)	Zn(1)-O(4)	2.685(3)
O(4)-La(1)-O(4)#2	119.988(4)	O(5)-La(1)-O(1)#3	136.36(9)
O(4)-La(1)-O(1)#5	68.44(13)	O(4)#2-La(1)-O(3)	74.02(13)
O(4)-La(1)-O(1)#4	134.18(13)	O(3)#1-La(1)-O(3)	107.55(10)
O(4)-La(1)-O(1)#3	72.19(12)	O(5)-La(1)-O(3)#1	68.67(9)
O(4)-La(1)-O(3)	50.21(13)	O(4)#1-La(1)-O(3)	154.61(13)
N(2)-Zn(1)-N(1)#7	112.61(18)	N(1)#7-Zn(1)-O(1)#7	79.73(16)
N(2)-Zn(1)-O(1)#7	110.93(17)	O(3)-Zn(1)-O(1)#7	168.79(15)
Symmetry transformations used to generate equivalent atoms: #1 -z+1,x-1/2,-y+1/2 ; #2 y+1/2,-z+1/2,-x+1 ; #3 x+1/2,-y+1/2,-z ; #4 z+1,x,y ; #5 -y+1,z+1/2,-x+1/2 ; #6 x,-y+1/2,z+1/2 ; #7 z+1/2,x,-y+1/2.			
2			
Ce(1)-O(5)	2.543(5)	Ce(1)-O(4)	2.549(2)
Ce(1)-O(4)#1	2.549(2)	Ce(1)-O(4)#2	2.549(2)
Ce(1)-O(1)#3	2.5711(19)	Ce(1)-O(1)#4	2.5711(19)
Ce(1)-O(1)#5	2.5711(19)	Ce(1)-O(3)#1	2.605(2)
Ce(1)-O(3)	2.605(2)	Ce(1)-O(3)#2	2.605(2)
Zn(1)-O(2)#6	1.995(2)	Zn(1)-N(2)	2.025(2)
Zn(1)-N(1)#7	2.073(2)	Zn(1)-O(3)	2.130(2)
Zn(1)-O(1)#7	2.165(2)	Zn(1)-O(4)	2.678(2)
O(4)#1-Ce(1)-O(4)	119.985(2)	O(5)-Ce(1)-O(1)#3	136.40(5)
O(4)-Ce(1)-O(1)#4	68.59(7)	O(4)-Ce(1)-O(3)#2	73.43(7)
O(4)-Ce(1)-O(1)#5	134.25(7)	O(3)#1-Ce(1)-O(3)	107.52(5)
O(4)-Ce(1)-O(1)#3	72.22(7)	O(5)-Ce(1)-O(3)	68.65(5)
O(4)-Ce(1)-O(3)	50.71(6)	O(4)-Ce(1)-O(3)#1	154.79(7)
N(2)-Zn(1)-N(1)#7	112.98(9)	N(1)#7-Zn(1)-O(1)#7	79.44(8)
N(2)-Zn(1)-O(1)#7	111.84(9)	O(3)-Zn(1)-O(1)#7	168.10(8)
Symmetry transformations used to generate equivalent atoms: #1 y+1/2,-z+1/2,-x+1 ; #2 -z+1,x-1/2,-y+1/2 ; #3 x+1/2,-y+1/2,-z ; #4 -y+1,z+1/2,-x+1/2 ; #5 z+1,x,y ; #6 x,-y+1/2,z+1/2 ; #7 z+1/2,x,-y+1/2.			
3			
Pr(1)-O(5)	2.526(5)	Pr(1)-O(4)#1	2.5309(18)
Pr(1)-O(4)#2	2.5310(18)	Pr(1)-O(4) #3	2.5310(18)
Pr(1)-O(1)#4	2.5574(18)	Pr(1)-O(1)	2.5575(18)
Pr(1)-O(1)#5	2.5575(18)	Pr(1)-O(3) #1	2.5956(18)
Pr(1)-O(3)#3	2.5956(18)	Pr(1)-O(3)#2	2.5956(18)
Zn(1)-O(2)#5	1.998(2)	Zn(1)-N(2)#6	2.024(2)
Zn(1)-N(1)	2.075(2)	Zn(1)-O(3)#6	2.1311(18)
Zn(1)-O(1)	2.1695(19)	Zn(1)-O(4)	2.674(2)
O(4)#1-Pr(1)-O(4)#2	119.972(3)	O(5)-Pr(1)-O(1)	136.33(4)
O(4)#3-Pr(1)-O(1)	68.74(6)	O(4)#3-Pr(1)-O(3)#1	72.88(6)
O(4)#1-Pr(1)-O(1)	134.57(6)	O(3)#1-Pr(1)-O(3)#2	107.27(5)
O(4)#2-Pr(1)-O(1)	72.40(6)	O(5)-Pr(1)-O(3)#2	68.41(4)

O(4)#1-Pr(1)-O(3)#1	51.12(6)	O(4)#1-Pr(1)-O(3)#3	154.60(6)
N(2)#6-Zn(1)-N(1)	113.08(9)	N(1)-Zn(1)-O(1)	79.57(7)
N(2)#6-Zn(1)-O(1)	112.03(8)	O(3)#6-Zn(1)-O(1)	167.92(7)

Symmetry transformations used to generate equivalent atoms: #1 y+1/2,-z+1/2,-x; #2 -x,y+1/2,-z+1/2; #3 -z+1/2,-x,y+1/2 ; #4 z,x,y ; #5 y,z,x ; #6 y,-z+1/2,x+1/2.

Table 2. (continued) Selected Bond Distances (Å) and Angles (º) for **1-8**

		4	
Sm(1)-O(4)#1	2.483(2)	Sm(1)-O(4)#2	2.483(3)
Sm(1)-O(4)#3	2.483(2)	Sm(1)-O(5)	2.485(5)
Sm(1)-O(1)#4	2.512(2)	Sm(1)-O(1)	2.512(2)
Sm(1)-O(1)#5	2.512(2)	Sm(1)-O(3)#1	2.565(2)
Sm(1)-O(3)#3	2.565(2)	Sm(1)-O(3)#2	2.565(2)
Zn(1)-O(2)#4	1.994(3)	Zn(1)-N(2)#6	2.026(3)
Zn(1)-N(1)	2.071(3)	Zn(1)-O(3)#6	2.146(2)
Zn(1)-O(1)	2.177(2)	Zn(1)-O(4)	2.663(2)
O(4)#1-Sm(1)-O(4)#2	119.922(6)	O(5)-Sm(1)-O(1)	136.23(6)
O(4)#2-Sm(1)-O(1)	69.28(8)	O(4)#3-Sm(1)-O(3)#1	71.80(8)
O(4)#3-Sm(1)-O(1)	135.31(8)	O(3)#3-Sm(1)-O(3)#1	106.74(6)
O(4)#1-Sm(1)-O(1)	72.77(8)	O(5)-Sm(1)-O(3)#1	67.92(6)
O(4)#1-Sm(1)-O(3)#1	51.82(8)	O(4)#2-Sm(1)-O(3)#1	153.99(8)
N(2)#6-Zn(1)-N(1)	113.31(11)	N(1)-Zn(1)-O(1)	79.55(10)
N(2)#6-Zn(1)-O(1)	113.07(11)	O(3)#6-Zn(1)-O(1)	167.13(9)

Symmetry transformations used to generate equivalent atoms: #1 -x+1/2,-y,z+1/2; #2 z+1/2,-x+1/2,-y; #3 -y,z+1/2,-x+1/2; #4 y,z,x; #5 z,x,y; #6 y+1/2,z,-x+1/2.

		5	
Eu(1)-O(4)#1	2.471(2)	Eu(1)-O(4)#2	2.471(2)
Eu(1)-O(4)#3	2.471(2)	Eu(1)-O(5)	2.480(5)
Eu(1)-O(1)	2.510(2)	Eu(1)-O(1)#4	2.510(2)
Eu(1)-O(1)#5	2.510(2)	Eu(1)-O(3)#2	2.564(2)
Eu(1)-O(3)#1	2.564(2)	Eu(1)-O(3)#3	2.564(2)
Zn(1)-O(2)#5	1.990(2)	Zn(1)-N(2)#6	2.026(3)
Zn(1)-N(1)	2.070(3)	Zn(1)-O(3)#6	2.142(2)
Zn(1)-O(1)	2.178(2)	Zn(1)-O(4)	2.661(2)
O(4)#1-Eu(1)-O(4)#2	119.909(6)	O(5)-Eu(1)-O(1)	136.22(5)
O(4)#3-Eu(1)-O(1)	69.35(7)	O(4)#3-Eu(1)-O(3)#1	71.57(7)
O(4)#1-Eu(1)-O(1)	135.45(8)	O(3)#2-Eu(1)-O(3)#1	106.59(6)
O(4)#2-Eu(1)-O(1)	72.88(7)	O(5)-Eu(1)-O(3)#2	67.78(5)
O(4)#1-Eu(1)-O(3)#1	51.99(7)	O(4)#2-Eu(1)-O(3)#1	153.83(8)
N(2)#6-Zn(1)-N(1)	113.55(11)	N(1)-Zn(1)-O(1)	79.26(9)
N(2)#6-Zn(1)-O(1)	113.25(10)	O(3)#6-Zn(1)-O(1)	167.00(9)

Symmetry transformations used to generate equivalent atoms: #1 -y+3/2,-z,x-1/2 ; #2 -x+3/2,-y+1,z+1/2 ; #3 -z+1/2,-x+1,y-1/2; #4 -z+1,x-1/2,-y+1/2 ; #5 y+1/2,-z+1/2,-x+1 ; #6 y,-z+1/2,x-1/2.

		6	
Gd(1)-O(4)#1	2.4627(19)	Gd(1)-O(4)#2	2.4628(19)

Gd(1)-O(4)#3	2.4628(19)	Gd(1)-O(5)	2.476(5)
Gd(1)-O(1)	2.4948(19)	Gd(1)-O(1)#4	2.4948(19)
Gd(1)-O(1)#5	2.4949(19)	Gd(1)-O(3)#1	2.5603(19)
Gd(1)-O(3)#2	2.5603(19)	Gd(1)-O(3)#3	2.5603(19)
Zn(1)-O(2)#4	1.993(2)	Zn(1)-N(2)#6	2.025(2)
Zn(1)-N(1)	2.068(2)	Zn(1)-O(3)#6	2.150(2)
Zn(1)-O(1)	2.1858(19)	Zn(1)-O(4)	2.664(2)
O(4)#1-Gd(1)-O(4)#2	119.866(6)	O(5)-Gd(1)-O(1)	136.07(5)
O(4)#1-Gd(1)-O(1)	69.54(6)	O(4)#2-Gd(1)-O(3)#1	71.40(6)
O(4)#3-Gd(1)-O(1)	135.96(7)	O(3)#1-Gd(1)-O(3)#2	106.35(5)
O(4)#2-Gd(1)-O(1)	73.14(6)	O(5)-Gd(1)-O(3)#1	67.56(5)
O(4)#1-Gd(1)-O(3)#1	51.93(6)	O(4)#1-Gd(1)-O(3)#2	153.33(7)
N(2)#6-Zn(1)-N(1)	113.79(9)	N(1)-Zn(1)-O(1)	79.17(8)
N(2)#6-Zn(1)-O(1)	113.54(8)	O(3)#6-Zn(1)-O(1)	166.90(8)

Symmetry transformations used to generate equivalent atoms: #1 -z+1/2,-x+1,y-1/2; #2 -x+1/2,-y+2,z+1/2; #3 -y+3/2,-z+1,x+1/2; #4 y-1/2,-z+3/2,-x+1; #5 -z+1,x+1/2,-y+3/2 ; #6 y-1,-z+3/2,x+1/2.

Table 2. (continued) Selected Bond Distances (Å) and Angles (º) for **1-8**

7			
Tb(1)-O(4)#1	2.443(3)	Tb(1)-O(4)#2	2.443(3)
Tb(1)-O(4)	2.443(3)	Tb(1)-O(5)	2.453(6)
Tb(1)-O(1)#3	2.483(3)	Tb(1)-O(1)#4	2.483(3)
Tb(1)-O(1)#5	2.483(3)	Tb(1)-O(3)#1	2.550(3)
Tb(1)-O(3)#2	2.550(3)	Tb(1)-O(3)	2.550(3)
Zn(1)-O(2)#6	1.985(3)	Zn(1)-N(2)	2.020(3)
Zn(1)-N(1)#7	2.066(3)	Zn(1)-O(3)	2.153(3)
Zn(1)-O(1)#7	2.186(3)	Zn(1)-O(4)	2.657(3)
O(4)#1-Tb(1)-O(4)	119.855(10)	O(5)-Tb(1)-O(1)#3	136.12(7)
O(4)-Tb(1)-O(1)#4	69.66(10)	O(4)#2-Tb(1)-O(3)	70.84(10)
O(4)-Tb(1)-O(1)#3	136.01(10)	O(3)-Tb(1)-O(3)#2	106.42(8)
O(4)-Tb(1)-O(1)#5	73.20(10)	O(5)-Tb(1)-O(3)#2	67.62(7)
O(4)-Tb(1)-O(3)	52.37(10)	O(4)-Tb(1)-O(3)#2	153.50(10)
N(2)-Zn(1)-N(1)#7	113.60(14)	N(1)#7-Zn(1)-O(1)#7	79.21(12)
N(2)-Zn(1)-O(1)#7	113.95(13)	O(3)-Zn(1)-O(1)#7	166.56(11)

Symmetry transformations used to generate equivalent atoms: #1 -z+1,x-1/2,-y+1/2 ; #2 y+1/2,-z+1/2,-x+1 ; #3 z+1/2,-x+3/2,-y ; #4 y+1,z,x-1 ; #5 -x+2,y+1/2,-z+1/2 ; #6 x-1/2,y,-z+1/2 ; #7 -z+1,-x+1,-y.

8			
Y(1)-O(4)#1	2.4176(14)	Y(1)-O(4)#2	2.4176(14)
Y(1)-O(4)	2.4176(14)	Y(1)-O(5)	2.435(3)
Y(1)-O(1)#3	2.4571(13)	Y(1)-O(1)#4	2.4571(14)
Y(1)-O(1)#5	2.4571(14)	Y(1)-O(3)#2	2.5409(14)
Y(1)-O(3)	2.5409(14)	Y(1)-O(3)#1	2.5409(14)
Zn(1)-O(2)#6	1.9860(15)	Zn(1)-N(2)	2.0215(15)
Zn(1)-N(1)#7	2.0665(16)	Zn(1)-O(3)	2.1540(14)
Zn(1)-O(1)#7	2.1931(14)	Zn(1)-O(4)	2.655(1)
O(4)#1-Y(1)-O(4)	119.806(6)	O(5)-Y(1)-O(1)#3	136.04(3)
O(4)-Y(1)-O(1)#3	69.88(5)	O(4)#1-Y(1)-O(3)	70.41(5)

O(4)-Y(1)-O(1)#5	136.42(5)	O(3)#1-Y(1)-O(3)	106.08(4)
O(4)-Y(1)-O(1)#4	73.42(5)	O(5)-Y(1)-O(3)#1	67.32(3)
O(4)-Y(1)-O(3)	52.63(4)	O(4)-Y(1)-O(3)#1	153.04(5)
N(2)-Zn(1)-N(1)#7	113.95(6)	N(1)#7-Zn(1)-O(1)#7	79.24(5)
N(2)-Zn(1)-O(1)#7	114.35(6)	O(3)-Zn(1)-O(1)#7	166.23(5)

Symmetry transformations used to generate equivalent atoms: #1 -y+1,z+1/2,-x+1/2 ; #2 -z+1/2,-x+1,y-1/2 ; #3 y-1/2,-z+1/2,-x ; #4 x+1/2,-y+3/2,-z ; #5 z+1/2,-x+1/2,-y+1 ; #6 x,-y+3/2,z+1/2 ; #7 z,-x+1/2,y-1/2.

10. Additional References

[1] APEX2, Data Collection Software Version 2.1-RC13, Bruker AXS, Delft, The Netherlands (2006).

[2] Cryopad, Remote momitoring and control, Version 1.451, Oxford Cryosystems, Oxford, United Kingdom (2006).

[3] SAINT+, Data Integration Engine v. 7.23a. Bruker AXS, Madison, Wisconsin, USA (1997-2005).

[4] G. M. Sheldrick, SADABS v. 2.01, Bruker/Siemens Area Detector Absorption Correction Program 1998, Bruker AXS, Madison, Wisconsin, USA.

[5] G. M. Sheldrick, SHELXS-97, Program for Crystal Structure Refinement, University of Göttingen (1997).

[6] G. M. Sheldrick, SHELXL-97, Program for Crystal Structure Solution, University of Göttingen (1997)